

# Software-based Interferometric Positioning

*Benoit Muth, Patrick Oonincx & Christian Tiberius*

## Introduction

This article discusses the revival of the interferometric positioning experiment with GPS signals that aims at measuring the three-dimensional vector between two stations. Such an experiment was carried out in the late seventies, the early days of the GPS system, almost simultaneously by two competing teams that had means, astronomic telescopes, without any common measure with those at stake in our setup. From a hardware point of view, the innovative aspect of this paper lies in the implementation of the experiment with software receivers. GNSS software receivers are attractive tools given the low price of the corresponding front-ends and the flexibility of receiver processing implementations in software.

From a positioning point of view, several reasons account for the re-discovery of this experiment. First, a differential positioning technique between two stations, such as relative positioning with GPS signals, originates from the field of interferometry. Secondly, beyond relative positioning with code measurements only, the use of precise carrier phase measurements for GNSS positioning also originates from the interferometry framework. The low price of the software receivers front-ends and the increased precision of the differential positioning techniques are the attractive features of the experiment.

## Interferometry

### Principles of interferometry

The interferometry framework consists here in setting two identical software receivers consisting each of an isotropic antenna, a radio front-end

collecting signals in the L1 band and a laptop as depicted in Figure 1, and located at both ends of an unknown baseline to observe simultaneously and independently several radio sources, i.e. several satellites. The unknown three-dimensional vector between the two antennas is called the interferometer baseline vector [1].



Figure 1: Signals were recorded simultaneously 9 December 2008, at two stations equipped with software receivers and located in the surroundings Den Helder, The Netherlands. Left: map (Google) indicating the baseline location, where the yellow pins indicate the two stations. Right: software receiver recording set-up at the Stoomweg station where the small antenna is positioned on top of the tripod.

When measuring the phase differences of the signals received at the two antennas from a specific source, the direction of the baseline vector can be determined relative to the direction of the source. If the baseline length can be ignored compared to the distance from the source to the baseline, the received signal is considered as a plane wave arriving to the antennas from the same direction, the signal paths are parallel and the product of the Time-Difference-Of-Arrival (TDOA) of the two signals by the speed of light equals the projection of the baseline vector on the direction of the source as in Figure 2. However for the interferometry with GNSS signals, this plane wave approximation cannot be applied to any baseline, given the distance of the satellites to the Earth. In the exact case the GNSS signal has a spherical propagation and the deviation from true plane waves is proportional to the square of the baseline length divided by the satellite's distances, which is taken into account in the linearized observation equations [1].

Interferometry is a technique that consists of studying the interferences created by the superposition of two waves. This technique has been applied

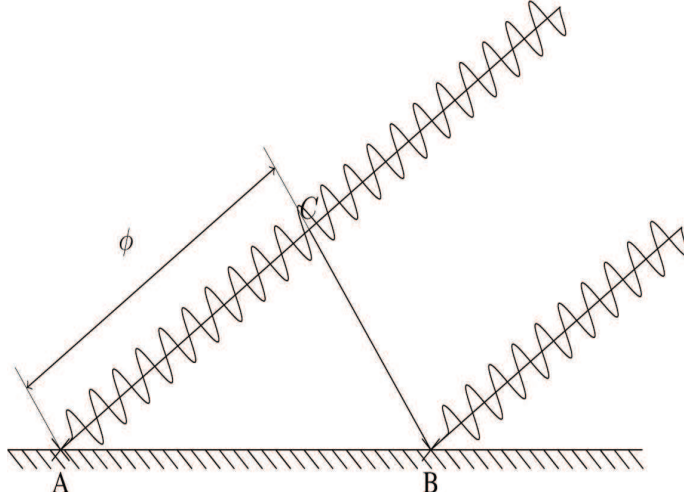


Figure 2: Interferometric configuration considering the plane wave approximation for the signal received from one source at the two stations A and B.

extensively in a variety of fields, e.g. astronomy, optics or plasma physics, also for positioning, first with signals from astronomic sources, second with GNSS signals [2]. Generally speaking, the TDOA of any two signals at the receiver can be measured with two types of observables: phase and group-delay observables. The simplified model of the phase observable  $\phi$  is

$$\phi(t) = \frac{2\pi f}{c} \mathbf{B}(\mathbf{t}) \cdot \mathbf{s} + \phi_{media}(t) + \phi_{instru}(t) + 2\pi A \quad (1)$$

where the phase  $\phi$  is in radians,  $f$  is the signal frequency and  $c$  the speed of light. In a chosen reference system  $\mathbf{B}$  is the baseline vector,  $\mathbf{s}$  the unit Line Of Sight vector from the reference point to the source and therefore  $\mathbf{B}(\mathbf{t}) \cdot \mathbf{s}$  is the projection of the baseline in the direction of the source. Next,  $\phi_{media}(t)$  and  $\phi_{instru}(t)$  are imprecisions of the observable respectively due to random short-term changes of the media, e.g. multipath, and of the instrumentation, e.g. clock errors.  $A$  is the integer number of carrier cycles called the ambiguity. The derivative of the phase  $\phi$  with respect to the angular frequency  $2\pi f$  is the interferometric group-delay

$$\tau(t) = \frac{1}{c} \mathbf{B}(\mathbf{t}) \cdot \mathbf{s} + \tau_{media}(t) + \tau_{instru}(t) \quad (2)$$

in seconds. These phase and group delay observables contain the whole baseline vector information and correspond in the case of GPS to the single-difference carrier phase and code observables respectively. Interferometric positioning, i.e. the computation of a baseline with single-differencing techniques has been achieved first with analogue hardware processing GPS

signals [2,3]. Next, the evolution of receiver technologies gave birth to radio front-ends specifically designed for GNSS software receivers. Means to collect experimental GNSS data could then be acquired for a few hundred euro. The opportunity to acquire such front-ends has been another motivation for reproducing the interferometric experiment in a Software Defined Receiver framework [4], where not only the TDOA but also the differential Doppler between the received signals were computed yielding a two-dimensional correlation map.

Interferometric positioning is a semi-codeless technique, since the structure of the spreading sequences is not needed to produce the observables. This property enables on one hand the use of satellites whose code structure is unknown to a particular receiver, e.g. Galileo in an early stage or the Chinese GNSS Compass. On the other hand, the spreading codes are convenient to assign the peaks in the integrated correlation to specific PRNs, determine the satellite geometry and compute the baseline. This is why raw code phase and Doppler estimates are computed in a standalone mode for all satellites in each data stream, before being differenced and matched to the interferometric code and Doppler observables. The baseline vector can be computed using group delay or phase observables that are best modeled into observation equations including terms due to various phenomena such as atmospheric effects for very precise applications and/or for very long baselines. In our case, these differential atmospheric effects can be neglected considering the baseline length. Accurate reference coordinates for one station lead to useable single-difference observation equations.

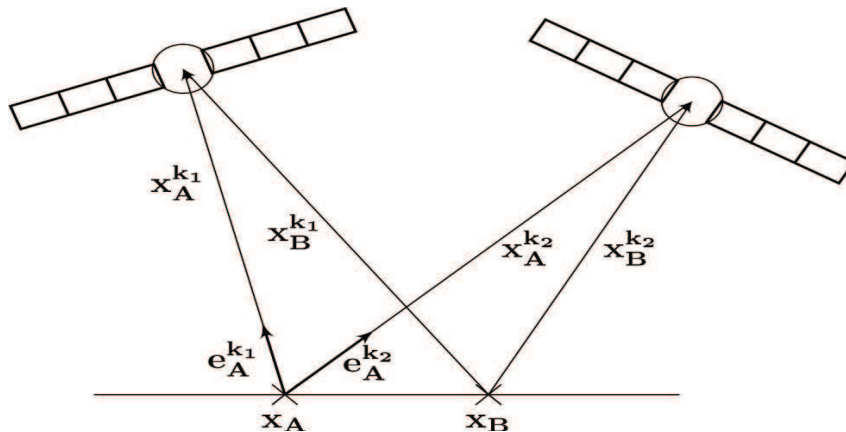


Figure 3: Configuration of satellites and receivers for GNSS interferometric positioning and GNSS relative positioning.

For one observation instant at stations A and B recording signals from the same satellite  $k$ , the single-difference equation for code observables reads

$$E [\Delta P_{AB}^k] = [ -\mathbf{e}_B^k \quad c ] \begin{bmatrix} \Delta \mathbf{x}_{AB}^k \\ \Delta \delta t_{AB} \end{bmatrix} \quad (3)$$

where  $\Delta P_{AB}^k$  is the vector of measured group delays,  $\mathbf{e}_B^k$  is the unit LOS vector from station  $B$  to satellite  $k$ ,  $\Delta \delta t_{AB}$  the single difference receiver clock error. The satellite clock error is absent from this equation where all terms correspond to differences between the receivers, or between the reference receiver and the satellite. The single-difference equation for phase observations  $\Delta p_{AB}^k$  contains the additional phase ambiguity  $\mathbf{A}_{AB}^k$ .

$$E [\Delta p_{AB}^k] = [ -\mathbf{e}_B^k \quad c \quad \lambda \mathbf{I} ] \begin{bmatrix} \Delta \mathbf{x}_{AB}^k \\ \Delta \delta t_{AB} \\ \mathbf{A}_{AB}^k \end{bmatrix} \quad (4)$$

where  $\Delta p_{AB}^k$  is the vector of measured phase difference,  $\mathbf{e}_B^k$  is the unit LOS vector from station  $B$  to satellite  $k$ ,  $\Delta \delta t_{AB}$  the single difference receiver clock error and  $\mathbf{A}_{AB}^k$  the single difference ambiguity [5]. These ambiguities can be left floating, though the float solution obtained with less than one minute of phase observations would be less precise than the baseline obtained with group-delays. In other words, with equipment enabling such short recording durations only, fixing the ambiguities is necessary to take advantage of the precision of the carrier phase measurements.

## Interferometric observables

### Received signal

In our study the GPS L1 raw data have been recorded with the Sparkfun GN3S front-end depicted at page 31 of this NL ARMS. that includes a magnetic patch antenna and a SiGe SE4110L GPS chip [6]. The analog part of the receiver downconverts the signal to an intermediate frequency  $f_{IF}$  of 4.1304 MHz, the analog-to-digital converter (ADC) produces samples at  $f_s$  equal to 16.3676 MHz that are delivered to a laptop through a USB connection and a driver only is needed to have a functioning receiver. However the recording duration is limited and the stability of our front-end exemplars is a cause for concern, as the signal's spectra have been observed at the time of the experiment, shifted and unbalanced, both to a severe extent. The sampled received signal  $x$  is the sum of all  $K$  satellite signals

arriving in A, having each its own PRN code, amplitude, Doppler frequency and Time-of-Arrival, plus a white Gaussian noise process  $n$  modeling the noise from the environment and the front-end.

### Cross-correlation

The cross-correlation function (CCF) of the two received signals yields a correlation map featuring peaks representing localized versions of the individual CCF of all received satellite signals present in the two data streams. These peaks can be best described by the auto-correlation function (ACF) of the transmitted GPS signal, which in turn can be approximated to the ACF of its one millisecond periodic PRN spreading code. Assuming the received signals have the same Doppler, their differential code phase can be found by maximising the sampled CCF of the discrete signals collected at the two stations

$$\hat{c}_{AB}[m] = \frac{1}{N_p} \sum_{n=0}^{N_p-|m|-1} s_A[n]s_B[n - |m|] \quad m \geq 0 \quad (5)$$

where  $N_p$  is the length of signals  $s_A$  and  $s_B$ . However the two receivers being far enough from each other and having unsynchronized, drifting, clocks, the signals received from one satellite most of the time have different Doppler frequencies at the two stations. The cross-correlation of the received signals is then maximal only for the differential code offset and the differential Doppler frequency. The sampled CCF  $c_{AB}[m, f]$  is computed iteratively after introducing bins corresponding to frequency shifts on the signal. The baseline length together with the sampling frequency impact the length of the correlation interval containing the received signal's energy. These quantities, as well as the total length of the experiment, influence the computational cost of the correlation operation. We chose an irregular frequency grid having more bins close to the IF frequency than far from it. Denoting  $\odot$  as the circular correlation operator using the DFT [6], the correlation  $c$  of one millisecond of data collected at A and B writes

$$c(\tau_{AB}, f_{AB}^d) = s_A(t, f) \odot s_B(t + \tau_{AB}, f + f_{AB}^d) \quad (6)$$

The CCF of two noisy GPS signals has a SNR far lower than the CCF of one received GPS signal and a clean replica. Consequently to detect the satellite's energy, we chose to non-coherently integrate the received signal's correlation over 1000 code periods. The cross-correlation of two frequency-shifted copies of the signals then yields a two-dimensional correlation map

containing all the TDOA and differential Doppler information of the signals received at the two stations.

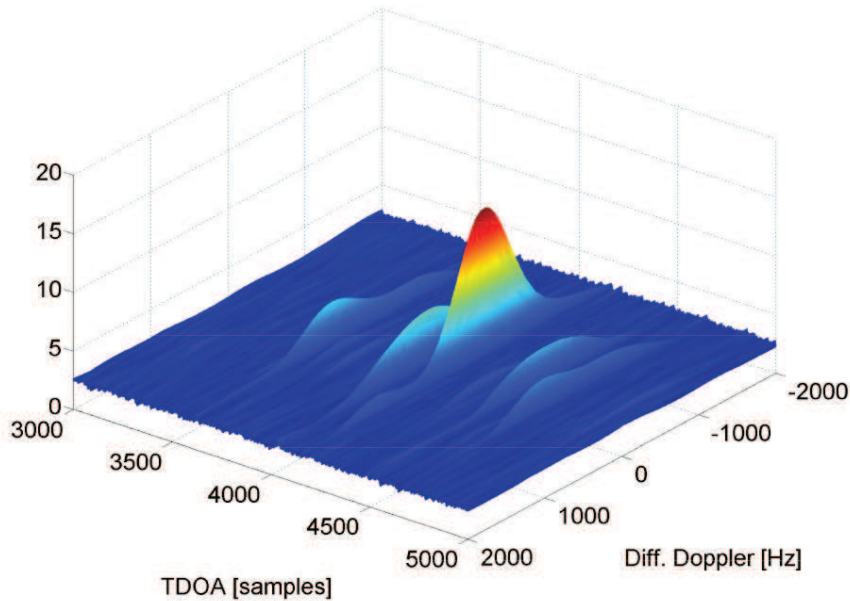


Figure 4: Region of a correlation map containing the received signals energy, obtained for a one second observation duration. Horizontally the map is parametrised by the TDOA and the differential Doppler, while the color-coded height corresponds to the correlation value. This figure shows peaks localised in time and frequency corresponding to the cross-correlation of the signals simultaneously received at the two stations. Outside the peaks region the correlation surface can be considered as flat.

## Measurements

The resolution of the differential measurements is limited by the dimensions of the correlation map, which is in turn conditioned by the computational cost of the correlation operations and the available processing memory. On one hand the sampling frequency drives the time resolution of the code phase observables. On the other hand the frequency resolution of the Doppler observables is constrained by the integration time as for the acquisition in a classical standalone receiver. The observables can then be refined in the time-domain by interpolating the correlation values in the detected frequency bin, resulting in TDOA estimates with better resolution. While TDOA measurements can be extracted from the correlation map, differential phase observables are more difficult to obtain and not considered here, since our hardware does not allow the production of these measurements.

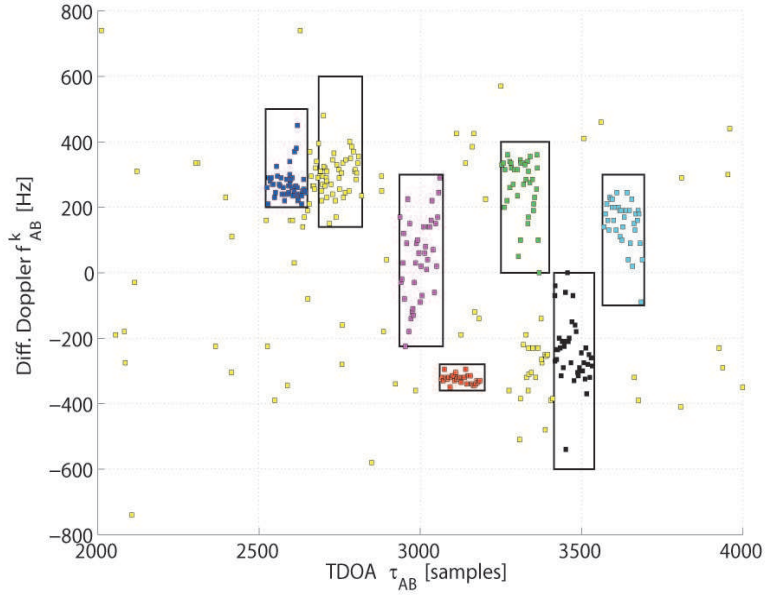


Figure 5: Differential code-Doppler observables obtained from 37 observation durations of one second each. Several color-coded clusters of points corresponding to different satellites can then be identified.

### Identification of satellites

The map of observables contains data clusters corresponding to visible but unknown satellites we identify thanks to their differential Doppler. Indeed the code-Doppler couples of all satellites in each data record can be computed separately with an open-loop processing that uses non-coherent integration and produced code phase and Doppler observables for each data stream. This open-loop processing is preceded by standard code and carrier acquisition steps, with increasingly fine frequency estimation stages. The sequential processing then uses integration to increase the sensitivity of the reception and yields at each recursion estimates for the code phase  $\hat{\tau}^k[n]$  and Doppler  $\hat{f}_k^d[n]$ . One correction is applied to compensate for the non-integer number of samples per code period and for the Doppler shift on the code sequence giving a new code phase  $\hat{\tau}^{k*}[n]$ . The strongest satellites in each data record were kept and those obviously unable to lock discarded. The satellite signal strengths are depicted in Figure 6.

Collecting the code phase and Doppler information for all satellites yields maps for both signals, which are differenced and brought back to

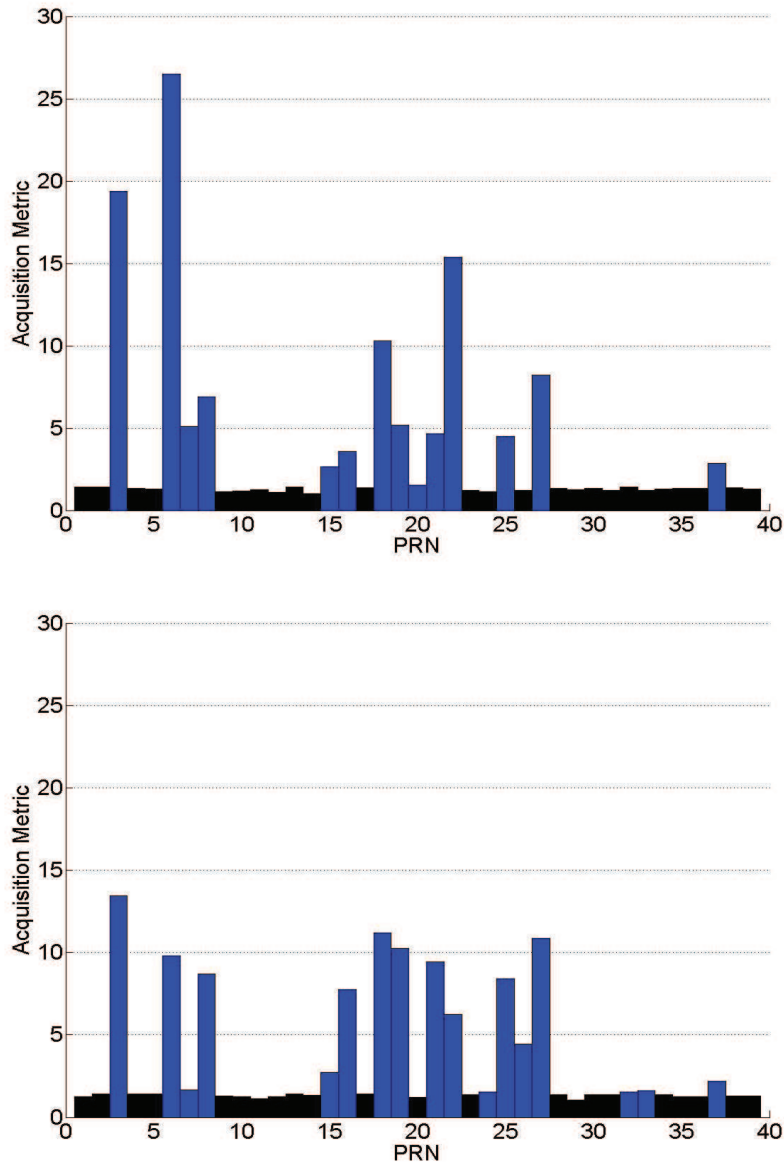


Figure 6: Acquisition metrics using non-coherent integration of ten milliseconds long signals recorded at the two stations, after correcting the initial start offset. The bottom plot shows a significant degradation in the received signal strength compared to the upper station. We link this phenomena to an anomaly in this specific exemplar of the front-end.

a one code period. These differential observables have a known PRN and then constitute a reference for those from the direct interferometry. The matching between the maps of observables from the interferometry and from the standalone processing, then the standalone observables, need only be precise enough to discriminate different satellites within a map.

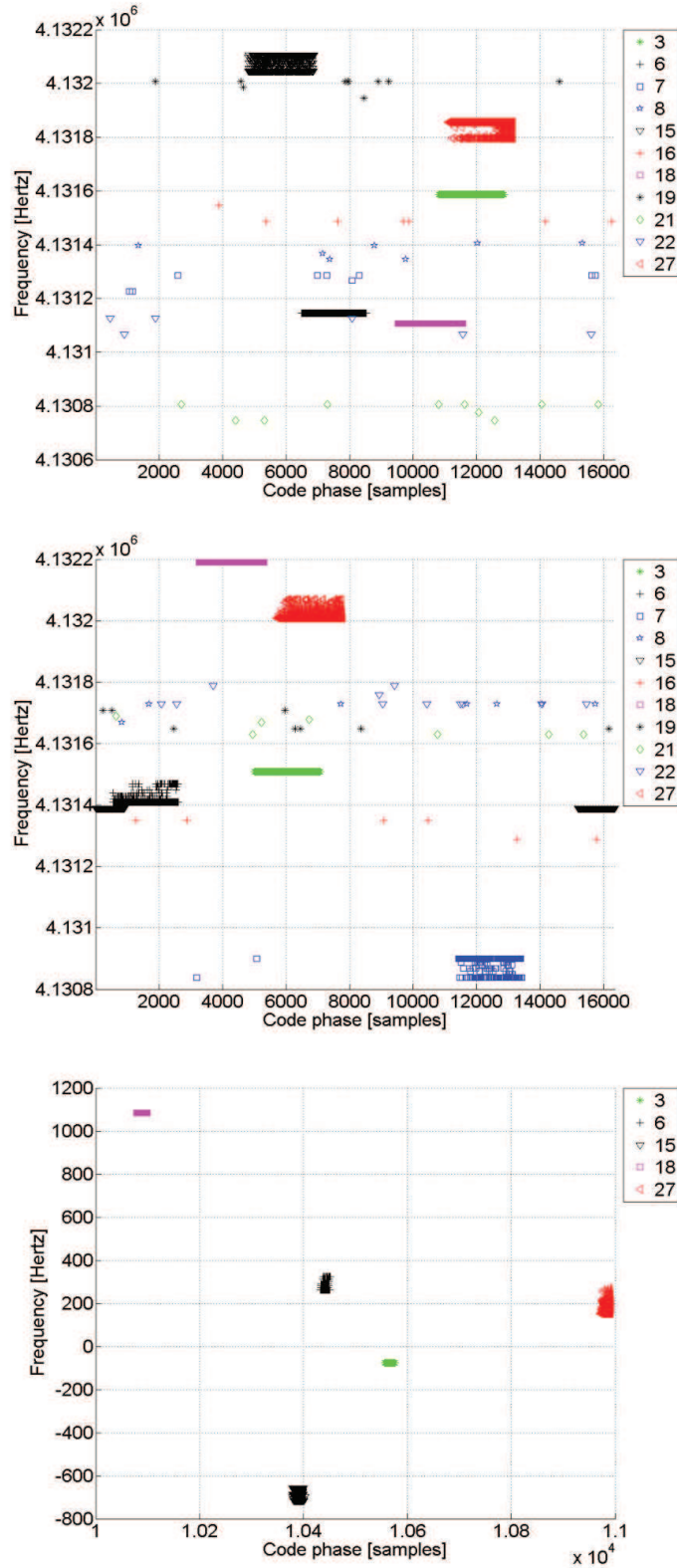


Figure 7: Code-Doppler results from the standalone processing at the two stations (top and middle) and differenced results for the strongest satellites (bottom) that is used as a reference for identifying the interferometric observables.

## Correction of the clocks

Each receiver is based on several clocks: the oscillator in the front-end and the laptop hardware clock, from which a signal time-tag is produced. Both laptop clocks were synchronised using a LAN connection to an Internet time server shortly before the experiment, and the recordings are triggered using the job scheduler on each laptop. Now, the different clocks are drifting causing difficult synchronisation of the records' start. The standalone closed-loop PLL and DLL processing at each receiver delivers prompt correlator outputs containing the navigation data. The correlator output sequences having a 1 kHz sampling rate can be cross-correlated, yielding a coarse estimate of the offset between the records' start. Long enough sequences should be taken to ensure common data bits and the estimation is repeated for several satellites adding reliability to the estimated value.

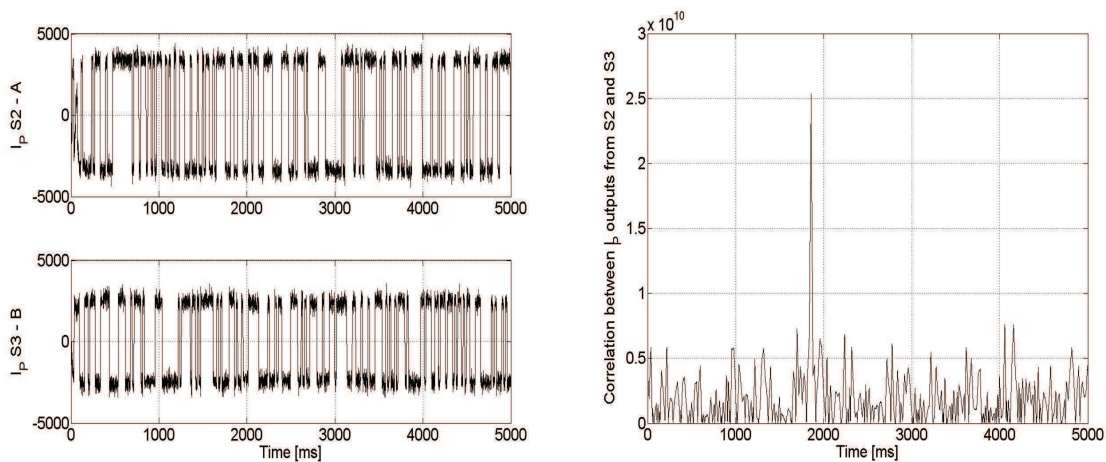


Figure 8: In-phase prompt correlation outputs at the two stations (left) and coarse estimated time-delay between the start of the records, resolution of one code period

Next, the offset is computed for all recordings in the measurement campaign and depicted in Figure 9, where it changes considerably in time, thus showing an anomaly in the analogue part of one of the software receivers.

## Conclusions

In this paper we presented a methodology to produce and identify differential code measurements used for interferometric positioning with GNSS signals. Having dealt with the synchronisation between the start of the

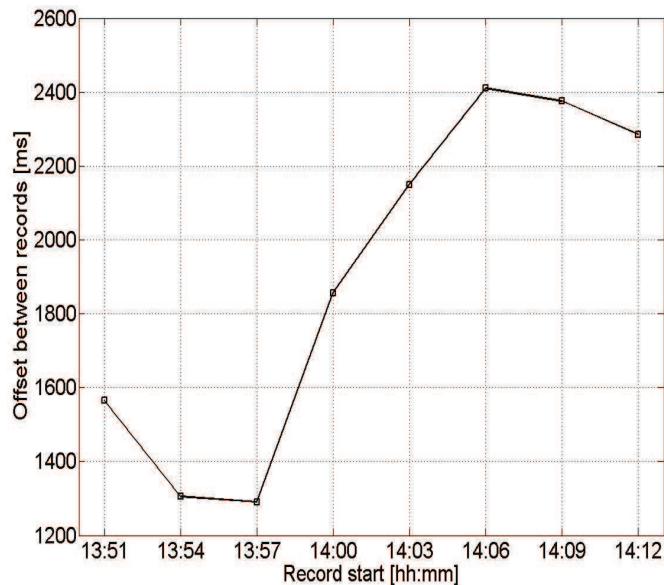


Figure 9: Differential clock offset for all signals recorded during the measurement campaign.

records, the processing of the raw data collected at two stations yields integrated cross-correlation maps. Processing both data streams separately enables the identification of the received satellite signals in the correlation maps. The whole experiment is then semi-codeless. The production of code measurements is well understood while the collection and processing of phase measurements, theoretically leading to a better baseline precision, remains challenging especially with the front-ends in our possession. Indeed, while the interferometric concept is straightforward and powerful, while the data collection is easy, the expected overall performance cannot reach a geodetic level given the low price of our equipment.

## References

- [1 ] G. Seeber, *Satellite Geodesy*, 2nd edition. Berlin/New York: de Gruyter, 2003.
- [2 ] C. C. Counselman and I. I. Shapiro, “Miniature interferometer terminals for earth surveying,” *Journal of Geodesy*, vol. 53, pp. 139-163, 1979.
- [3 ] P. F. MacDoran, “Satellite Emission Radio Interferometric Earth

Surveying Series - GPS Geodetic System,” *Bull. Geodesy*, pp. 117-138, 1979.

- [4 ] B. Muth, P. Oonincx and C. Tiberius, “GNSS Software-based Interferometry,” *European Journal of Navigation*, vol. 7, pp. 10-16, August 2009.
- [5 ] P.Misra and P. Enge, *Global Positioning System - Signals, Measurements, and Performance*, 2nd edition. Lincoln, (Massachusetts): Ganga-Jamuna Press, 2006.
- [6 ] D. Akos, K. Borre, N. Bertelsen, P.Rinder and S. Jensen, *A single-frequency software-defined GNSS receiver*, Birkhäuser, 2007.

